One-Component Molecular Glass Photoresists for EUV Lithography

CNF Project Number: 386-90
Principal Investigator(s): Christopher Kemper Ober
User(s): Yusuke Otsubo

Affiliation(s): Materials Science and Engineering, Cornell University
Primary Source(s) of Research Funding: JSR Corporation
Contact: c.ober@cornell.edu, yo237@cornell.edu
Primary CNF Tools Used: Zeiss Supra SEM, ASML 300C DUV stepper, ABM contact aligner

Abstract:

Extreme ultraviolet (EUV) lithography has entered into high volume manufacturing (HVM) phase in 2019. However, meeting the increased requirements for the photoresists still remains a challenge. As the feature size decreases, it is becoming more difficult to meet the requirements using conventional organic polymer-based chemically amplified resists (CAR). In this context, development of new photoresist material platforms with high resolution maintaining high sensitivity and low roughness is highly demanded. Our group has previously shown that molecular glass photoresist system has the excellent potential as a high-resolution photoresist platform. We are currently attempting to improve the performance of molecular glass photoresist by introducing photoacid generator (PAG) moieties into the resist molecules, making it completely one-component system. In this report, our preliminary results of deep ultraviolet (DUV) patterning with newly developed one-component molecular glass photoresists are described.

MATERIALS

Summary of Research:

Introduction. EUV lithography has already been in HVM phase. Throughout the next decade, a resolution of sub-10 nm half pitch (HP) will be the industry-wide target. In the era of sub-10 nm HP, which is comparable with polymeric materials, it is obvious that conventional CAR system reaches the technical limitation.

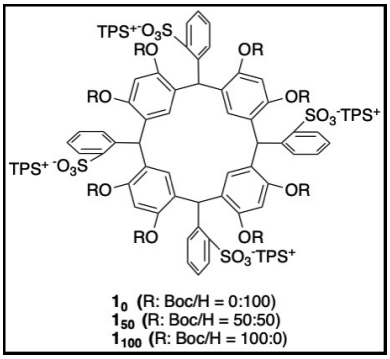

Figure 1: Chemical structures of the molecular glass photoresists used in the study.

Our group has previously reported utilization of amorphous small organic molecules, known as molecular glasses, as new photoresist platform [1,2]. Smaller, well-defined size of molecular glass resists compared to CAR was shown to be advantageous for achieving high resolution and low roughness patterning. However, perfect uniformity in component has yet to be achieved, as the previous systems required PAG as additive. In this work, we are attempting to develop completely one-component molecular glass photoresists, assuming that perfect uniformity in component as well as in size will give more homogeneous films, and therefore high resolution and low roughness patterning.

Material Design and Synthesis. Photoresist material has to meet several requirements including solubility, film forming ability and etch resistance. Especially for molecular glasses, which has low molecular weight and therefore higher tendencies to crystalize than polymers, additional care for crystallization should be paid because it will cause pattern deformation in lithography. To prevent crystallization, it is important to keep glass-transition temperature (T_g) much higher than temperature in post- and pre-exposure baking steps.

We have previously demonstrated that resorcin[4]arene-based molecular glass photoresists show high T_g due to its rigid and phenolic structures [2]. Herein we designed and synthesized novel one-component molecular resists by introducing PAG moieties on the rim of resorcin[4] arene core in varying substitution degree (Figure 1). The sulfonate groups were covalently bounded to the core in order to limit the diffusion of generated photoacid. The synthesis can be done only in three steps from reasonable commercially available reagents and basic laboratory techniques. This would allow feasible industrial scale production at low cost.

The synthesized photoresists could be dissolved in gamma-butyl lactone (GBL), a common spin-coating solvent regardless of their degree of substitution.

The solutions in GBL remained clear and did not give any precipitation even after one months at room temperature.

Photolithographic Performance Evaluation. Thin films could be fabricated by spin-coating 5 wt% GBL solutions onto unprimed 4-inch silicon wafers. The formed films did not show any obvious cracks. DUV exposure was performed using ABM contact aligner equipped with 248 nm filter and the exposed films were developed using isopropanol (IPA). Obtained pattered films were observed with optical microscope (Figure 2). Although much more improvement needs to be made, the microscopic images showed vague positive-tone patterns obtained without any PAG as additive. These preliminary results encourage us to explore one-component molecular glass system more.

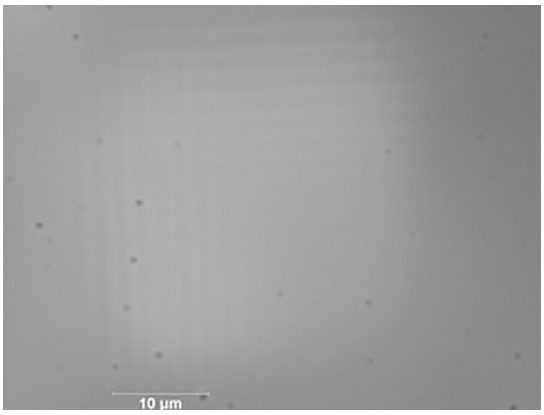

Figure 2: Optical microscope images of patterned film with 150. Prebake: 150°C/60s; Exposure: 20 mJ/cm^2; Development: isopropanol 120s.

Conclusions and Future Steps:

Novel resorcin[4]arene-based one-component photoresist materials have been successfully synthesized. They showed good film formation and positive-tone patterning ability with DUV exposure. Further improvements to obtain high contrast pattern from both material and process sides is underway.

References:

[1] J. Dai, S. W. Chang, A. Hamad, D. Yang, N. Felix, C. K. Ober Chem. Mater. 2006, 18, 3404-3411.

[2] S. W. Chang, R. Ayothi, D. Bratton, D. Yang, N. Felix, H. B. Cao, H. Deng, C. K. Ober J. Mater. Chem. 2006, 16, 1470-1474.

Amorphous Bi-Ti-O Thin Film Dielectrics

CNF Project Number: 1400-05
Principal Investigator(s): R. Bruce van Dover
User(s): Rita Sun

Affiliation(s): Materials Science and Engineering, Cornell University
Primary Source(s) of Research Funding: Air Force Office of Scientific Research
Contact: vandover@cornell.edu, rs2537@cornell.edu
Primary CNF Tools Used: FilMetrics

Abstract:

Amorphous bismuth titanate (Bi-Ti-O) composition spread thin films were fabricated using off-axis reactive RF co-sputtering. Continuous compositional spreads allow for high-throughput analysis techniques. Optical reflectometry and profilometry were applied on reference single-element samples and Bi-Ti-O composition spreads to generate composition maps. Metal contacts were deposited on the samples for dielectric properties measurement. Dielectric constant, dissipation factor and current-voltage characteristics reveal the potential of amorphous Bi-Ti-O thin films as a novel dielectric for application in capacitive circuit elements.

Summary of Research:

The investigation of new candidate thin film dielectric materials has been of great importance in capacitive circuits applications for various electronic devices. A good dielectric material exhibits a high dielectric constant and a low dissipation factor that gives low leakage current. These features increase the effective capacitance of the capacitive circuit elements. Besides, amorphous thin films are preferable over polycrystalline materials, since they are generally cheaper and easier to fabricate, especially on modern circuitry that has nanoscale features. Polycrystalline dielectrics are also expected to show a lower breakdown field than that of amorphous dielectrics due to the presence of grain boundaries. [1]

Amorphous bismuth titanate (Bi-Ti-O) thin films can be considered as a potential candidate thin film dielectric material. Crystalline $Bi_4Ti_3O_{12}$ has been reported to show a high dielectric constant and low dissipation factor [2]. Furthermore, to investigate composition-dependent trends of dielectric properties, a composition-spread technique for thin film growth can be applied for high-throughput analysis of a wide range of compositions [3].

In this work, amorphous Bi-Ti-O composition spread thin films were synthesized by off-axis reactive RF magnetron sputtering to investigate the composition-dependence of dielectric properties.

Optical reflectometry was performed on Bi-Ti-O composition spread thin films by FilMetrics in the Cornell NanoScale Science and Technology Facility (CNF). Profilometry was performed on calibration Bi-O and Ti-O samples to help obtain composition maps of samples. The thickness of Bi-Ti-O thin films was measured by profilometry. An array of silver contacts was deposited on Bi-Ti-O thin films as top electrodes for the characterization of dielectric properties. Silver dot contacts were deposited by thermal evaporation in CNF. Capacitance, dissipation factor and current-voltage characteristics were measured using a high-throughput setup which consists of an LCR meter and an electric probe with an automatic stage.

Figure 1 shows the capacitance map as a function of the sample position (Bi-rich region on the left, Ti-rich region on the right) on the Bi-Ti-O thin film. The data shown was measured at 10 kHz, while values that were too high or too low to be realistic are shown in white color. High capacitance values can be observed in the central region and the Ti-rich side of the Bi-Ti-O composition spread thin film.

Figure 2 and Figure 3 illustrate the dielectric constant and the dissipation factor of Bi-Ti-O as a function of composition. It can be seen that Bi-Ti-O thin film with a Bi:Ti ratio of roughly 1:1 appears to exhibit a high dielectric constant while maintaining a low dissipation factor.

Figure 4 shows the maximum breakdown field as a function of composition. Addition of Ti in $Bi_{1-x}Ti_xO_y$ up

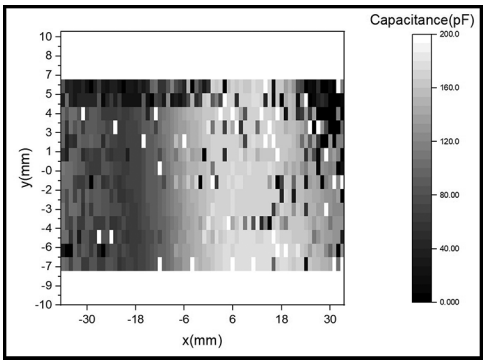

Figure 1: Capacitance map of Bi-Ti-O thin film as a function of sample position (Bi-rich region on the left, Ti-rich region on the right).

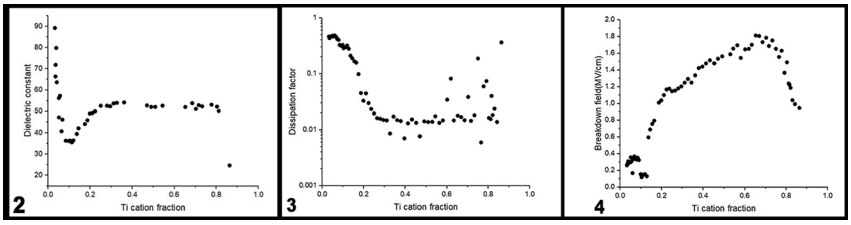

Figure 2, left: *Dielectric constant of Bi-Ti-O as a function of Ti cation composition.* ***Figure 3, middle:*** *Dissipation factor of Bi-Ti-O as a function of Ti cation composition.* ***Figure 4, right:*** *Breakdown field of Bi-Ti-O as a function of Ti cation composition.*

to x around 0.7 increases the breakdown field of the sample, which can result in a good maximum stored charge of approximately 8 $\mu C/cm_2$.

Conclusions and Future Steps:

The dielectric properties of amorphous Bi-Ti-O composition spread thin films were examined. Amorphous Bi-Ti-O was found to show good potential as a dielectric material. However, using the profilometry data to characterize the composition as a function of the sample position is a rough approximation. More accurate data can be obtained from optical reflectometry, which can be further used to characterize the refractive index of samples. Furthermore, laser spike annealing can be performed on the samples to form stable and metastable phases in addition to the as-deposited amorphous phase [4], which can be enable the investigation of the effect of different crystalline phases on dielectric properties of Bi-Ti-O thin films.

References:

[1] Naoi, T. A., Paik, H., Green, M. L., and Dover, R. B. V. (2015). Dielectric properties of amorphous Zr-Al-O and Zr-Si-O thin films. Journal of Advanced Dielectrics, 05(01), 1550010. doi: 10.1142/s2010135x15500101.

[2] Alfonso, J., Olaya, J., Bedoya-Hincapié, C., Toudert, J., and Serna, R. (2014). Annealing Effect on the Structural and Optical Properties of Sputter-Grown Bismuth Titanium Oxide Thin Films. Materials, 7(5), 3427-3434. doi: 10.3390/ma7053427.

[3] van Dover, R. B., Schneemeyer, L. F., Fleming, R. M., and Huggins, H. A. (1999). A high-throughput search for electronic materials-thin-film dielectrics. Biotechnology and bioengineering, 61(4), 217-225.

[4] Bell, R. T., Jacobs, A. G., Sorg, V. C., Jung, B., Hill, M. O., Treml, B. E., and Thompson, M. O. (2016). Lateral Temperature-Gradient Method for High-Throughput Characterization of Material Processing by Millisecond Laser Annealing. ACS combinatorial science, 18(9), 548-558.

Three-Dimensional Printing with Silica Cages

CNF Project Number: 1645-08
Principal Investigator(s): Tobias Hanrath
User(s): Jen-Yu Huang

Affiliation(s): Robert F. Smith School of Chemical and Biomolecular Engineering, Cornell University
Primary Source(s) of Research Funding: National Science Foundation
Contact: th358@cornell.edu, jh2486@cornell.edu
Primary CNF Tools Used: ZEISS Supra and Ultra SEMs, Leica supercritical dryer

Abstract:

Material scientists have now developed an extensive library of nano-sized building blocks, offering a vast panel of properties (optic, magnetic, plasmonic, catalytic, etc.). Nevertheless, combining these building blocks for the realization of multifunctional materials while controlling their structure from the nano- to the micro- and all the way to the macroscale still remains an open challenge in order to fully exploit their potential. In parallel, new material processing techniques such as 3D printing technologies are emerging for the fabrication of macroscopic highly engineered parts and devices. In this work, newly discovered silica nanocages are combined with digital light processing 3D printing technique for the rapid fabrication of mesoporous parts with arbitrary shapes and tunable internal structures. Complementary strategies are then deployed for the implementation and deliberate positioning of various functionalities throughout 3D printed objects with high control on the microstructure and macroscopic architecture of the superstructures. This approach paves the road for innovative device concepts and designs, that will benefit from the unique properties of nanomaterials and from the micro-and macroscale manufacturing capability of 3D printers.

Summary of Research:

In this work, silica cages were made compatible with digital light processing 3D printing, through our reported photoresponsive ligand on inorganic core (PLIC) concept [1].

Making use of the printed cage-based mesoporous materials, we developed a hitherto unknown internal 3D printing approach. Here, the porosity of an already printed 3D part serves as a scaffold for the subsequent printing of a second 3D material directly within the first. To demonstrate this concept, we printed a second metal structure within the pores of the first silica structure. As illustrated in Figure 1, a 3D block of silica cages was first printed as described before and then soaked for 30 minutes in a solution of silver nitrate (0.1 M in 10:1 v/v ethanol:toluene), and two photoinitiators, namely TPO (0.05 M) and Darocur 1173 (0.5 M). In this case, TPO acts as a sensitizer for Darocur 1173, which serves as the electron donor for the reduction of Ag^{+} to Ag^{0}.

A light pattern was then projected in the form of three lines to locally reduce silver, which remained embedded in the original 3D silica block (Figure 1d-f). The 3D printing of a second, more active material within a 3D printed mesoporous silica block opens a whole new scope of opportunities. Through this approach, the two materials are entangled with each other, which means that the structure of the scaffold or host material will influence the structure and therefore properties of the guest material.

As an example, deliberately varying the porosity of the silica host could allow to tune the electrical conductivity along the metal lines. Furthermore, the entanglement of the two materials also means that interactions between them such as charge transport, are possible and may even benefit from their high interfacial area. This approach can readily be extended to a large variety of materials offering a wealth of unique properties.

For instance, printing two different catalytic materials within a porous silica scaffold could result in a highly tunable platform with controlled symmetry and flux for tandem catalysis applications. The whole 3D printing toolbox can thereafter be put to practice for the positioning of active centers within the host scaffold with a great degree of freedom.

References:

[1] Huang, J.-Y. et al. Three-Dimensional Printing of Hierarchical Porous Architectures. Chem. Mater. acs.chemmater.9b02761, doi:10.1021/acs.chemmater.9b02761 (2019).

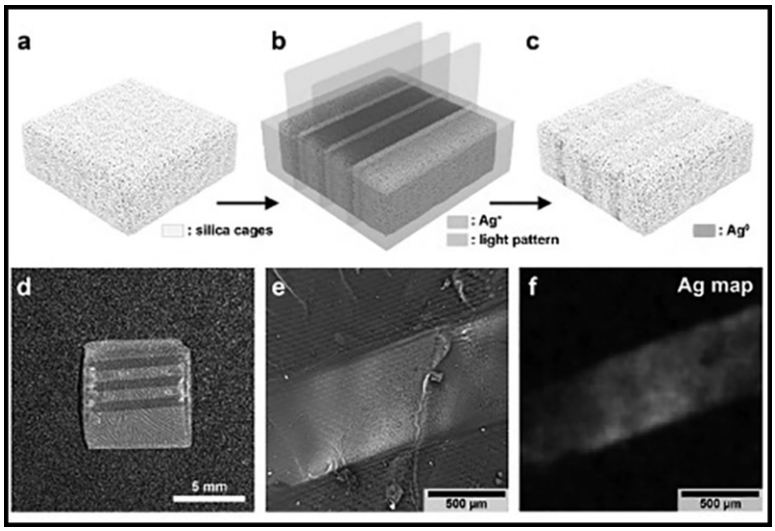

Figure 1: a-c, Illustration of the process of printing silver within a primary part printed with porous silica cages. First, a block of silica cages without additional functionalization is printed (a). The block is immersed in a solution of silver nitrate and photoinitiators. A light pattern in the shape of lines is then projected onto this block (b), resulting in the localized reduction of Ag^+ ions into Ag^0 (c). d, Photograph of the resulting block of silica cages exhibiting three lines of metallic silver. Backscattered electron-based SEM image (e) and EDS map (f) of a silver line embedded in the porous silica matrix.

Nanometer-Scale Area-Selective Formation of Polymer Brushes

CNF Project Number: 1757-09

Principal Investigator(s): Christopher Kemper Ober[2]

User(s): Yuming Huang[2], Hai Tran[1,2]

Affiliation(s): 1. Chemical and Biomolecular Engineering, 2. Materials Science and Engineering; Cornell University

Primary Source(s) of Research Funding: National Science Foundation

Contact: cko3@cornell.edu, yh839@cornell.edu

Website: https://ober.mse.cornell.edu/index.html

Primary CNF Tools Used: E-beam resist spinners, JEOL 9500, FilMetrics F50-EXR, Oxford 81 etcher, Zeiss Ultra SEM, optical microscope

Abstract:

The topological control of mixed polymer brushes can be realized via multi-steps surface-initiated polymerizations on a pattern fabricated by e-beam lithography, which is known for its fine resolution and precision. Patterned binary polymer brushes were produced on silicon wafers by area-selective deposition of two different initiators, using patterned e-beam resists as the masks. As a result, "nano-spikes" made of rod brushes were formed, surrounded by soft coil brushes. This platform has unique dual properties and thus can be used in various applications such as cytoskeleton mimicry and molecular recognition.

MATERIALS

Summary of Research:

Introduction. Polymer brushes are polymer chains that have one end covalently bonded to a substrate, such as a silicon wafer. Due to the unusual molecular arrangements, polymer brushes have demonstrated interesting surface properties and thus has been one of the main research focus in polymer science [1]. Potential applications such as metal oxide surface functionalization, optoelectronics, and medical diagnosis have been studied in the past decades. However, there is an increasing need for location-specific functionalization of these metal oxide surfaces as patterning techniques advances in the lithography industry. As such, incorporating e-beam lithography with the vapor phase surface-initiated polymerization can be a possible solution to the aforementioned demands.

Previously we have reported a new approach to nano-pattern rod-like polymer brushes with high persistence length using the equipment in Cornell NanoScale Facilities (CNF). This year we have made further advancement by incorporating our knowledge in combining rod-coil polymer brushes in a single system, which will provide enhanced phase separation and unique mechanochemical surface properties [2]. This report provides a novel pathway in fabricating nano-patterned rod-coil mixed polymer brushes on a silicon wafer, which will result in surfaces with dual properties, chemical functionality, and responsive behavior under different stimulations.

Fabrication. The mixed polymer brushes were patterned on a silicon wafer by multi-steps fabrication process and area-selective deposition of surface-bound initiators for polymerizations.

E-beam Resist Mask Preparation. Patterned e-beam resist mask (~150 nm) was prepared through JEOL 9500. The sample was then etched ~ 10 nm using Oxford 81 etcher to remove residual debris in the unmasked area.

Synthesis of the Rod Brushes. The deposition of a silane initiator on the treated substrate was carried out in a closed chamber under vacuum and elevator temperature. The initiator was allowed to vaporize and thus reacting with the exposed metal oxide surfaces. Afterward, the resist mask was removed by organic solvents. Subsequently, surface-initiated ring-opening polymerization of poly-*y*-benzyl-*L*-glutamate (PBLG), a rod-like polymer, was synthesized under vacuum and elevated temperature.

Synthesis of the Coil Brushes. The deposition of α-bromoisobutyryl bromide (BiBB) functionalized silane initiator was deposited onto the remaining unreacted area under similar conditions, followed by surface-initiated atom-transfer radical polymerization of poly(*N*-isopropylacrylamide) (PNIPAM), obtaining a thermo-responsive coil polymer brushes with low persistence length.

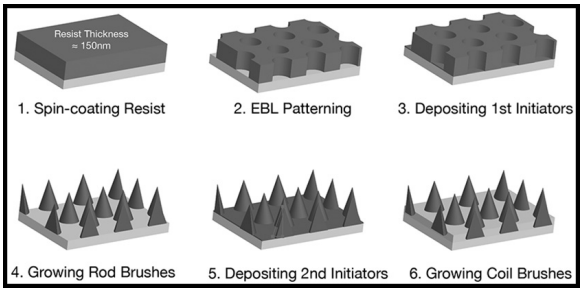

Figure 1: Schematic illustration of the fabrication process.

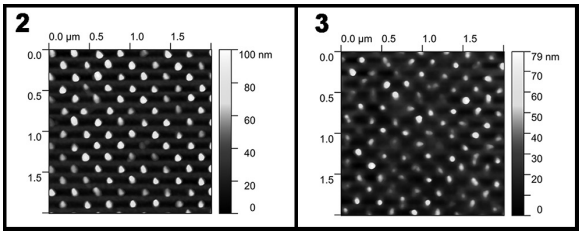

Figure 2 left: *AFM image of the patterned PBLG rod brushes.*
Figure 3, right: *AFM image of the mixed PBLG-PNIPAM brushes.*

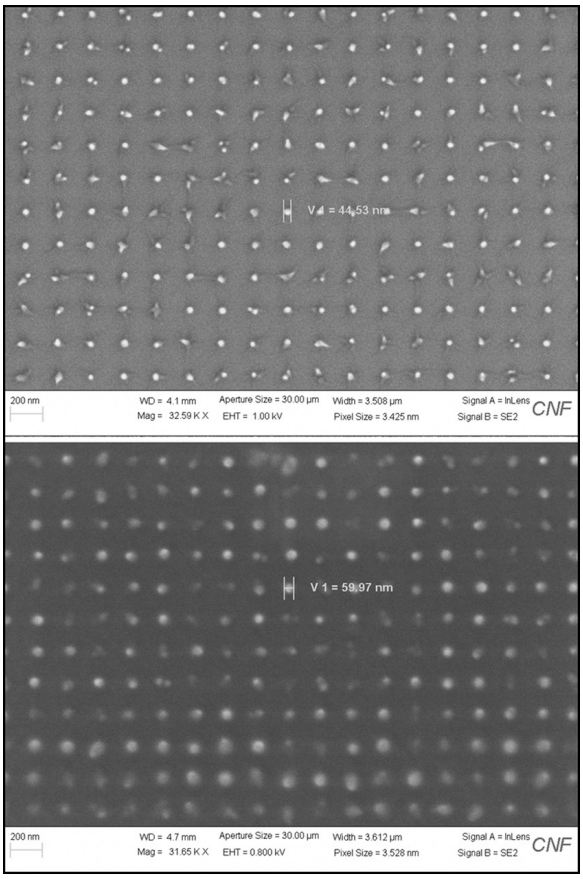

Figure 4: SEM images of the PBLG brushes (top) without PNIPAM and (bottom) with PNIPAM brushes.

A schematic illustration of the whole fabrication process is shown in Figure 1.

Characterization and Results:

The e-beam resist thickness was measured by FilMetrics F50-EXR. The patterned e-beam resist was examined using Zeiss Ultra SEM. The patterned PBLG rod brushes were characterized using atomic force microscopy (AFM) for height measurement (Figure 2), and Zeiss Ultra scanning electron microscopy (SEM) for topological analysis. The resulting surfaces with mixed rod-coil brushes were analyzed with AFM (Figure 3) and SEM (Figure 4) to compare the differences.

In conclusion, we demonstrated a process for precisely control the spatial arrangement of mixed rod-coil polymer brushes. In the near future, we plan to examine how the addition of thermo-responsive PNIPAM brushes in the system would affect the surface

properties. We also plan to explore the use of these surfaces for biological applications, such as cell membrane support and molecular recognition.

References:

[1] Chen, W. L.; Cordero, R.; Tran, H.; Ober, C. K., 50th Anniversary Perspective: Polymer Brushes: Novel Surfaces for Future Materials. Macromolecules 2017, 50 (11), 4089-4113.

[2] Tran, H.; Zhang, Y.; Ober, C. K., Synthesis, Processing, and Characterization of Helical Polypeptide Rod-Coil Mixed Brushes. ACS Macro Lett 2018, 7 (10), 1186-1191.

Nanotube Transistor Arrays on a TEM Substrate

CNF Project Number(s): 2486-16, 2858-19
Principal Investigator(s): Jonathan S. Alden
User(s): Jonathan S. Alden, Joshua S. Alden

Affiliation(s): Esper Biosciences, Inc.; McGovern Center, Cornell University
Primary Source(s) of Research Funding: National Institutes of Health, Esper Biosciences, Inc.
Contact: jonathan.alden@gmail.com, ja698@cornell.edu
Primary CNF Tools Used: Low pressure chemical vapor deposition (LPCVD) furnaces (oxide, nitride), Autostep i-line stepper, ABM contact aligner, SC4500 evaporators, Oxford 80 RIE

Abstract:

We use photolithography to fabricate nanotube transistor devices on substrates with thin nitride windows, which can be imaged using transmission electron microscopy (TEM). Our device architecture permits us to characterize a given nanotube both electrically, and by high-resolution TEM. In low-dimensional systems, such as nanotubes, where nanoscale surface and defect structure can have profound influences on the electrical properties, we expect this combined nanoscale imaging and electrical characterization to yield insights that will inform the design of nanoscale sensors.

Summary of Research:

The study of low-dimensional materials, such as carbon nanotubes, graphene, and molybdenum disulfide, has been an area of growing interest over the past decades, in part due to their promise as molecular sensors. Due to their one-to-few-atom thickness, the properties of such materials often depend sensitively on surface adsorbates, substrate-surface interaction and defect structure. Improving sample cleanliness, for example, enabled the first observations of spin-orbit coupling in carbon nanotubes [1] and, more recently, the fractal quantum Hall effect, known as Hofstadter's butterfly, in graphene [2]. In order to understand these nanoscale structures and subsequently design improved sensors, a device architecture is needed that combines the atomic-level characterization afforded by TEM with the electronics characterization ability enabled by a gated, transistor-like geometry. We demonstrate that we can produce arrays of gated nanotube sensors devices, with reasonably high yield that can be characterized afterwards by TEM. Our design also keeps parasitic capacitance from our electrodes to the highly resistive silicon substrate low enough to enable electronic measurements of our transistors at MHz bandwidth.

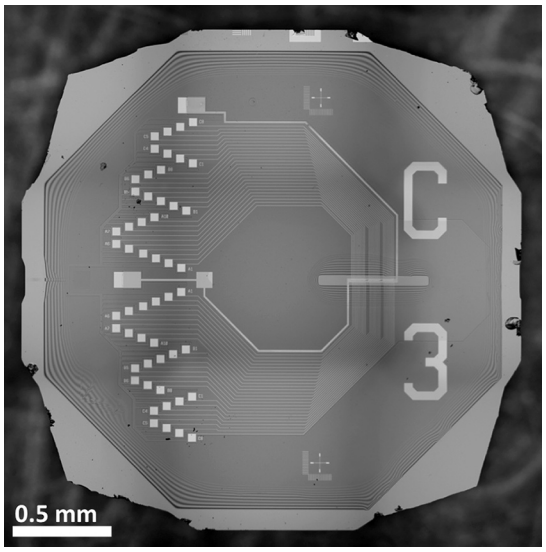

Figure 1: Optical image of microfabricated TEM grid with 26 pairs of source-drain electrodes, a top gate, and a thin nitride window for TEM imaging after top-gate is removed via chemical etching.

We fabricate nanotube devices on TEM grids using a combination of photolithography and standard nanotube growth and transfer techniques [3]. Figure 1 shows one of such devices, having 26 source-drain electrode pairs and two top gates. Between a few of the electrode pairs are individual nanotubes, which have been transferred prior to the deposition of a gate dielectric, and top-gate. The device fabrication involves using nine masks to define the various structures, which have been designed to yield nanotube devices with good gating characteristics, as well as low capacitive coupling between nearby electrodes.

The outline of the fabrication procedure is as follows. We begin by using low pressure chemical vapor deposition (LP CVD) to deposit the low-stress nitride on a 300 μm-thick silicon substrate, which will ultimately become our TEM window. We later deposit electrodes, and use

backside alignment followed by reactive ion etching (RIE) to expose rectangles on the back of the wafer which will later be used for a potassium hydroxide (KOH) through-etch. Arrays of parallel nanotubes are grown by CVD on a separate quartz substrate, coated with poly(methyl methacrylate) (PMMA), lifted off with KOH, and transferred onto the device substrate [3], where unwanted areas are patterned and etched using RIE. We use atomic layer deposition (ALD) to deposit a gate dielectric, after which we pattern and evaporate a gold top-gate. The surface is then coated with a KOH protection layer, and the devices are placed in hot KOH, which etches the silicon exposed on the back, to both release individual grids and to etch the silicon away from behind the nitride window. Later, the nanotube devices will be imaged through this window using TEM. The protection layer is then removed, and the grids are cleaned with oxygen plasma. Our fabrication process typically yields at least one electrically-connected, gated nanotube on 75% of the TEM grids.

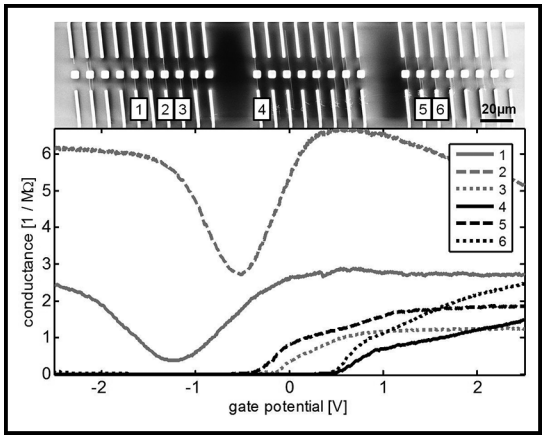

Figure 2: Upper: Scanning electron microscope image of nanotubes between source-drain electrodes, passing over thin nitride windows. Lower: Corresponding conductance measurements as a function of top gate voltage showing six conducting nanotubes with varying characteristics.

Figure 2 shows an SEM image of nanotubes patterned between the source-drain electrode pairs, imaged prior to top-gate deposition. The squares in the center are thin nitride windows for low-background TEM imaging. After completion of the device fabrication, these nanotubes are characterized electrically, shown in the lower portion of Figure 2. All of these nanotubes can be gated to have resistance lower than 1MΩ (50kΩ/μm) showing that they have a low defect density, and good coupling to the top gate. Nanotubes 1 and 2 can be seen to be metallic, while nanotubes 3-6 are semiconducting.

Furthermore, we can probe the electrical characteristics at high speeds in the megahertz (MHz) range. Previous research has shown that single charge fluctuations in a dielectric can be detected by semiconducting carbon

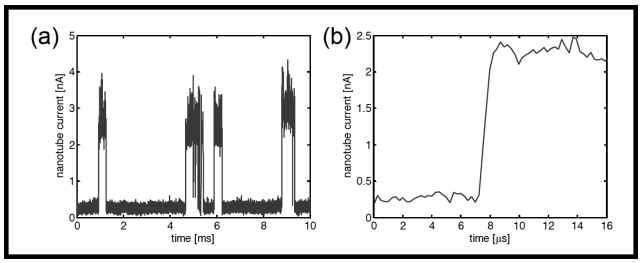

Figure 3: High-speed measurement of nanotube random telegraph signal showing (a) fluctuations in nanotube current and (b) measured rise time of less than 1 μs.

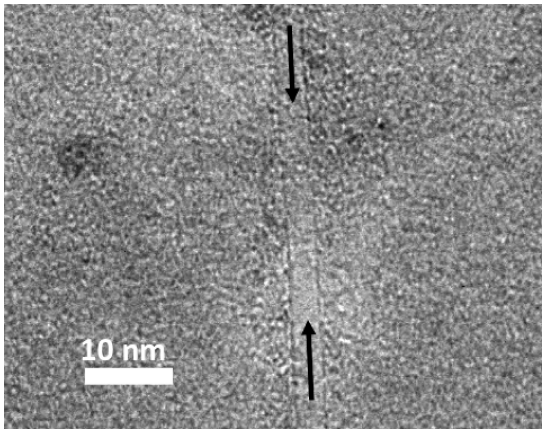

Figure 4: TEM image of a nanotube imaged through a thin nitride window, after top-gate removal.

nanotubes as random telegraph signals [4]. As shown in Figure 3, our devices are also capable of measuring such signals, but at higher speeds with rise times less than 1 μs. After characterizing the nanotubes electronically, we can etch away the gold top-gate, and image them by TEM to determine, for example, the nanotube diameter. Figure 3 shows one such nanotube, which can be seen to be single-walled (single dark lines running parallel to the arrows), and 4 nm in diameter (the width between those lines).

Conclusions and Future Steps:

In principle, our fabrication procedure can be applied to many different CVD-grown low-dimensional materials with only minor modifications, and may lead to the development of improved nanoscale sensors capable of high-speed molecular sensing.

References:

[1] F. Kuemmeth, et al., Nature 452 448-452 (2008).

[2] C. R. Dean, et al., Nature 497, 598-602 (2013).

[3] L. Jiao, et al., J. Am. Chem. Soc. 130, 12612-12613 (2008).

[4] T. Sharf, et al., Nano Lett. 14 (9) 4925-4930 (2014).

Antifouling Topographies to Combat Microbial Biofilms

CNF Project Number: 2505-16

Principal Investigator(s): Dacheng Ren[1,2,3,4]

User(s): Huan Gu[1,2]

Affiliation(s):1. Biomedical and Chemical Engineering, 2. Syracuse Biomaterials Institute, 3. Department of Civil and Environmental Engineering, 4. Department of Biology; Syracuse University, Syracuse, 13244 New York, USA

Primary Source(s) of Research Funding: National Institutes of Health (NIH), National Science Foundation (NSF)

Contact: dren@syr.edu, hugu@syr.edu

Website: https://renlab.syr.edu/

Primary CNF Tools Used: Heidelberg mask writer DWL2000, ABM contact aligner, Plasma-Therm UNAXIS 770 deep silicon etcher, MVD 100

Abstract:

Bacteria can adhere and develop multicellular structures (known as biofilms) on medical devices, which are the primary cause of hospital-acquired infections (HAI) and biofouling. Once mature biofilms are established, they are hard to eradicate, leading to the persistence of biofilm-mediated medical challenges. In this project, we aim to develop a strategy to address these challenges using biocompatible shape memory polymers (SMPs) with defined surface topography. The surface topography is introduced onto the surface of SMPs using photolithography and soft lithography. This strategy can prevent bacterial adhesion and remove mature biofilms on-demand, and therefore, providing prolonged antifouling properties. By challenging these new antifouling surfaces with *Pseudomonas aeruginosa* biofilms, these topographies demonstrate 99.9% biomass reduction compared to the static and flat controls. Similar potent antifouling effects are also observed against biofilms of *Staphylococcus aureus* and a uropathogenic strain of *Escherichia coli*. The data included in this report has been published in the Journal of ACS Applied Materials and Interfaces [1].

Summary of Research:

To fabricate well-defined surface topography on SMPs, we used poly(dimethylsiloxane) (PDMS) surfaces with complementary topography as molds (Figure 1). These PDMS surfaces were created using photolithography and soft lithography by following the protocol described by Hou, et al. [2]. In detail, the configuration of the patterns was designed using the software L-Edit (Tanner Research, Monrovia, CA, USA) to create hexagonal shapes with side length (L) of 5, 10, 15, 20, 30, 40, or 50 μm and inter-pattern distance (D) of 2, 5, 10, 15, or 20 μm.

This design was first written onto a photomask using a photomask writer (Heidelberg Mask Writer - DWL2000) and then transferred onto silicon wafers coated with photoresist S1813 using the ABM contact aligner. The hexagonal holes on silicon wafers were etched to obtain approximately 10 μm deep features using a Plasma-Therm Unaxis 770 deep silicon etcher.

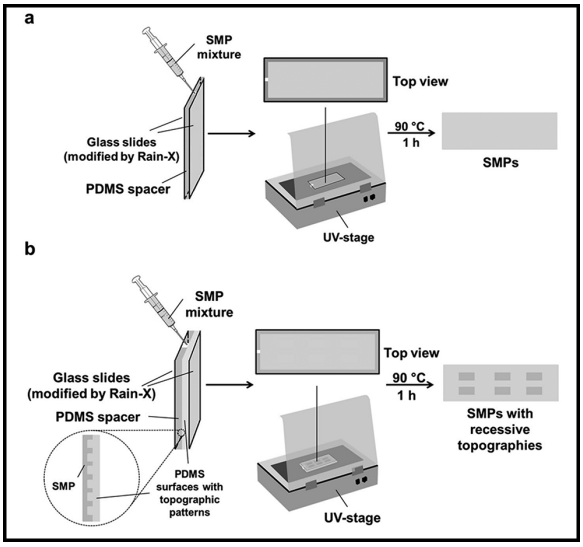

Figure 1: Schematic illustration of the process for preparing SMPs without (a) or with (b) surface topography.

To minimize PDMS residues in each round of soft lithography, silicon wafers were coated with (tridecafluoro-1,1,2,2,-tetrahydrooctyl)trichlorosilane (FOTS) prior to use as templates. Silicon elastomer mixtures (base : cure agent (wt/wt) = 10 : 1; Sylgard® 184, Sigma-Aldrich, St. Louis, MO, USA) were applied onto the silicon wafers and polymerized at 60°C for 24 h. PDMS surfaces with recessive hexagonal patterns were then gently peeled off and used as molds.

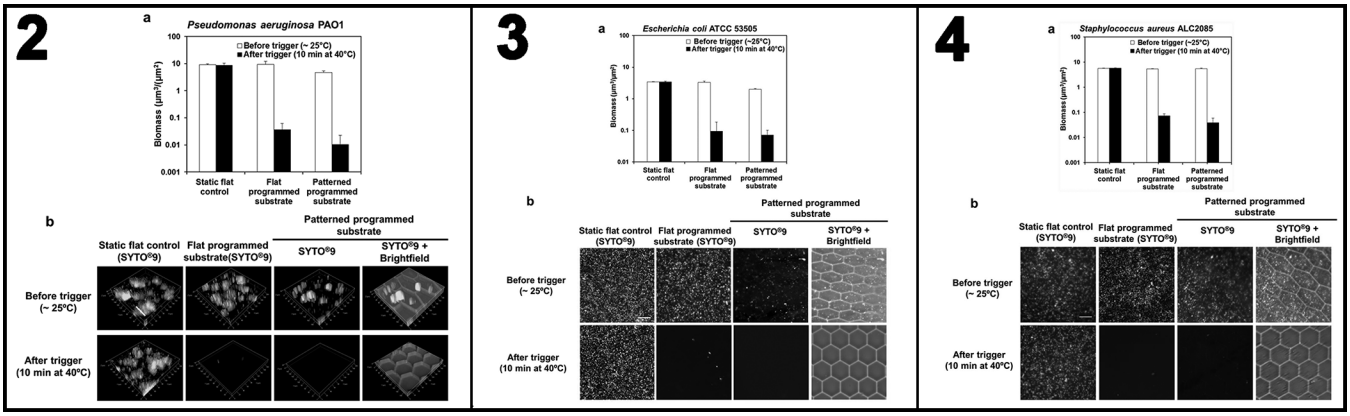

Figure 2, left: *Effects of static flat control and programmed substrates on the biofilm formation and mature biofilms of* P. aeruginosa *PAO1. Figure 2 shows the biomass (a) and representative fluorescence images (b) of* P. aeruginosa *PAO1 biofilms on different surfaces before and after trigger (10 min incubation at 40°C) (Bar = 50 μm) [1]. (Reproduced with permission from the Journal ACS Applied Materials and Interfaces.)* ***Figure 3, middle:*** *Effects of static flat control and programmed substrates on the biofilm formation and mature biofilms of* E. coli *ATCC53505. Figure 3 shows the biomass (a) and representative fluorescence images (b) of* E. coli *ATCC53505 biofilms on different surfaces before and after trigger (10 min incubation at 40°C) (Bar = 50 μm) [1]. (Reproduced with permission from the Journal ACS Applied Materials and Interfaces.)* ***Figure 4, right:*** *Effects of static flat control and programmed substrates on the biofilm formation and mature biofilms of* S. aureus *ALC2085. Figure 4 shows the biomass (a) and representative fluorescence images (b) of* S. aureus *ALC2085 biofilms on different surfaces before and after trigger (10 min incubation at 40°C) (Bar = 50 μm) 1]. (Reproduced with permission from the Journal ACS Applied Materials and Interfaces.)*

The SMP used in this study was synthesized by mixing t-butyl acrylate (tBA), poly(ethylene glycol) n dimethacrylate (PEGDMA), and photoinitiator 2,2-dimethoxy-2-phenylacetophenone (DMPA) (wt:wt:wt = 9:1:0.04). Flat or topographically patterned substrates were prepared by injecting the mixture between two glass slides with a 1 mm thick PDMS spacer using a syringe, being pre-polymerized under 365 nm UV irradiation for 10 min, followed by a thermal post-cure for 1 h at 90°C to maximize the conversion of monomers [3] (Figure 1). We programmed the shape change of SMPs by incubating dog bone shaped flat or topographically patterned substrates at 50°C for 5 min and then gradually stretching using a manual stretcher to 1.5 times of the original length. This temporary shape was fixed via approximately 5 min cooling at room temperature. We triggered shape recovery by incubating these SMP substrates with their temporary shape in pre-warmed 0.85% NaCl for 10 min at 40°C. Flat static control (samples that do not undergo shape change when heated) were also prepared.

By comparing the biomass of 48 h *P. aeruginosa* PAO1 on the three different surfaces that are flat static controls, flat and topographically patterned programmed surfaces, recessive hexagonal patterns were found to significantly prevent biofilm formation with 50.9 ± 7.2% and 51.9 ± 7.3% reduction in biomass compared to that on flat programmed substrates and static flat control, respectively ($p < 0.001$ for both, one way ANOVA adjusted by Tukey test; Figure 2a). No significant difference was found between static flat controls and flat programmed substrates (both around 9 $\mu m^3/\mu m^2$; $p = 0.93$). Shape recovery induced movement of recessive hexagonal patterns triggered more profound effects on removing the established biofilms. For instance, the biomass on topographically patterned programmed substrates was 0.01 ± 0.01 $\mu m^3/\mu m^2$ after shape recovery. This represents a 469-fold reduction of biomass compared to the biomass before shape recovery (4.7 ± 0.7 $\mu m^3/\mu m^2$), and 909-fold reduction compared to the 48 h *P. aeruginosa* PAO1 biofilm biomass (9.1 ± 0.8 $\mu m^3/\mu m^2$) on static flat controls without topographic patterns and shape change. These results were obtained by quantifying fluorescence images using COMSTAT4 (Figure 2b). Similar results were observed in preventing the biofilm formation and removing mature biofilms of two other microorganisms, *E. coli* and *S. aureus* (Figures 3 and 4).

In summary, we developed new antifouling surfaces based on shape memory triggered changes in surface topography. This strategy was found effective for the prevention and removal of established biofilms of multiple species. Future studies are needed to understand the underlying mechanism and develop biocompatible polymers for *in vivo* use with tailored temperature and duration of heating to achieve multiple cycles of shape change.

References:

[1] Gu, H., Lee, S. W., Buffington, S. L., Henderson, J. H., and Ren, D. On-Demand Removal of Bacterial Biofilms via Shape Memory Activation. ACS Appl Mater Interfaces 8, 21140-21144, doi:10.1021/acsami.6b06900 (2016).

[2] Hou, S., Gu, H., Smith, C., and Ren, D. Microtopographic Patterns Affect *Escherichia coli* Biofilm Formation on Poly(dimethylsiloxane) Surfaces. Langmuir, doi:10.1021/la1046194 (2011).

[3] Yakacki, C. M., Willis, S., Luders, C., and Gall, K. Deformation limits in shape-memory polymers. Adv Eng Mater 10, 112-119, doi:DOI 10.1002/adem.200700184 (2008).

[4] Heydorn, A., et al. Quantification of biofilm structures by the novel computer program COMSTAT. Microbiology-Uk 146, 2395-2407 (2000).

Encapsulation of Photocathodes in Two-Dimensional Materials

CNF Project Number: 2584-17

Principal Investigator(s): Melissa A. Hines

User(s): William J.I. DeBenedetti

Affiliation(s): Department of Chemistry and Chemical Biology, Cornell University

Primary Source(s) of Research Funding: Center for Bright Beams, an NSF-funded Science and Technology Center (STC), National Science Foundation

Contact: Melissa.Hines@cornell.edu, wjd74@cornell.edu

Website: http://hines.chem.cornell.edu

Primary CNF Tools Used: SC4500 odd-hour evaporator, YES CV200RFS oxygen plasma asher

Abstract:

We are developing a new technique for encapsulating highly reactive photocathodes in an atomically thin membrane that protects them from oxidation and degradation without affecting their photoemission properties or chemical purity.

MATERIALS

Summary of Research:

Photocathodes are materials that eject electrons under illumination. By their very nature, high-performance photocathodes must be made from materials that lose electrons easily — in other words, materials that are easily oxidized. For example, many photocathodes are either coated with alkali metals (e.g., Cs/GaAs) or comprised of alkali metals (e.g., Cs_3Sb). This presents a technical challenge, as exposure to even trace amounts of O_2 or H_2O will destroy or degrade the photocathode. For highest performance, the photocathodes must also be atomically flat and extremely homogeneous.

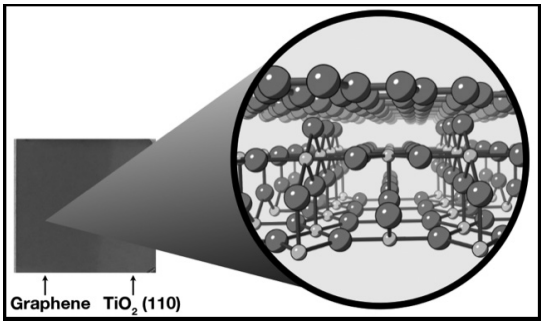

Figure 1: Optical image of TiO_2(110) with single-layer graphene on left side. The inset is a model of single-layer graphene on TiO_2(110).

To meet these challenges, we are developing a technique to produce a graphene-encapsulated photocathode. The key challenge in this project is ensuring that every step of the fabrication leaves no residue on the surface, as even monolayer levels of contamination could significantly reduce photoelectron transmission and beam brightness.

In the first step of fabrication, commercial two-dimensional materials, which are grown on a copper foil, are coated with a thin gold layer in the SC4500 thermal/e-beam evaporator. The two-dimensional material on the backside of the copper foil is then removed using 100W of oxygen plasma in the YES oxygen plasma asher. The copper foil is then removed with an aqueous etchant, allowing the graphene side of the gold-coated graphene to be adhered to a low energy substrate. The gold film is then removed by a second aqueous etch.

Deposition and Characterization of ALD Dielectric Materials for Metal-Insulator-Semiconductor AlGaN/GaN High Electron Mobility Transistors

CNF Project Number: 2684-18

Principal Investigator(s): Fatemeh Shahedipour-Sandvik

User(s): Benjamin McEwen

Affiliation(s): SUNY Polytechnic Institute, College of Nanoscale Science and Engineering

Primary Source(s) of Research Funding: Army Research Laboratory

Contact: sshahedipour-sandvik@sunypoly.edu, mcewen@sunypoly.edu

Primary CNF Tools Used: Oxford FlexAL ALD, Woollam spectroscopic ellipsometer

Abstract:

We continue our investigation of atomic layer deposition (ALD) for gate dielectric materials in AlGaN/GaN metal-insulator-semiconductor high electron mobility transistors (MISHEMTs). Al_2O_3, Si_3N_4, and SiO_2 were each tested. Pre- and post-deposition processes are found to greatly affect the quality of the dielectric and the dielectric/semiconductor interface. In particular, deposition of dielectric material as the first step in the fabrication process flow was found to be important. All devices fabricated with dielectric deposited after ohmic metallization exhibited high leakage currents and poor gate control. This presents a problem for Al_2O_3 MISHEMTs, since the Al_2O_3 has a relatively limited thermal budget and degrades at the temperatures necessary for ohmic metallization of GaN (~850°C).

MATERIALS

Summary of Research:

The next generation of (Al)GaN power switches will likely require MIS gates in order to operate as normally-off devices with low leakage and high gate swing. Adding a gate dielectric however, complicates the process flow as additional considerations for stability of the dielectric during subsequent processing must be made, and the additional dielectric/semiconductor interface may contain a high density of interface trap states (D_{it}), leading to issues such as high dynamic on resistance (R_{ON}) and premature breakdown.

To determine the effect of forming a gas (95% N_2/5% H_2) anneal on the Al_2O_3/GaN interface, unintentionally doped (UID) GaN was grown on c-plane sapphire using metal-organic chemical vapor deposition (MOCVD) — 20 nm of Al_2O_3 was deposited using the Oxford FlexAL ALD system at CNF; the substrate was maintained at 300°C during the deposition.

Temp (°C)	1 min	10 min	20 min
600	X		X
475		X	
350	X	X	X

Table 1: Forming gas annealing conditions applied to Al_2O_3 after deposition.

After the deposition, samples were annealed in forming gas for a range of temperatures and times, as outlined in Table 1. MIS capacitors were subsequently fabricated, and the conductance method was used to extract the D_{it}. The D_{it} of the samples annealed at 350°C for 10-20 min was found to be over an order of magnitude less than that of the sample annealed at 600°C for 20 min and approximately half an order of magnitude less than the samples with as-deposited material, annealed at 350°C for 1 min, annealed at 475°C for 10 min, and annealed at 600°C for 1 min.

This indicates that annealing in forming gas for long times at lower temperatures is beneficial, while the material starts to degrade at higher temperatures. As ohmic metallization temperatures for GaN are ~ 850°C, this means Al_2O_3 must be deposited after the ohmic metallization [1].

To compare the necessary ohmic-first Al_2O_3 MISHEMTs with dielectric-first Si_3N_4 and SiO_2 MISHEMTs (these materials have high thermal budget), MISHEMTs were fabricated, using the Oxford FlexAL ALD system at CNF to deposit all dielectric materials; ~ 15 nm of each material was deposited, as measured using the Woollam spectroscopic ellipsometer at CNF.

As shown in Figure 1, in all cases, several orders of magnitude reduction in gate leakage current relative to a Schottky-gated HEMT was observed. However, the sample with Al_2O_3 gate dielectric (deposited after ohmic metallization) exhibited poor gate control, and instead showed a high I_{DS} regardless of the applied V_{GS} (Figure 2). It is believed that this is due to a highly defective and/or contaminated interface between the dielectric and semiconductor, imparting a high fixed positive surface charge, making it impossible to deplete the 2DEG channel before dielectric breakdown [2].

In order to potentially recover the GaN surface and improve the quality of the dielectric/semiconductor interface, surface cleaning treatments were performed on GaN; using X-ray photoelectron spectroscopy (XPS), it was found that a cleaning procedure consisting of consecutive NH_4OH, HCl, and HF resulted in the lowest surface coverage of carbon and oxygen on the GaN [2]. This cleaning procedure was applied to Al_2O_3/AlGaN/GaN MISHEMT devices prior to dielectric deposition.

After ohmic contact metallization, samples were cleaned with NH_4OH, HCl, and HF immediately before being loaded in the Oxford FlexAL ALD chamber at CNF; 8 nm of Al_2O_3 was deposited at 300°C. Completed devices exhibited more gate control than devices fabricated in the same run with only acetone/IPA clean prior to Al_2O_3 deposition, but high I_{OFF} ~ 190 mA/mm was measured at V_{DS} = 10 V, compared to I_{ON} ~ 340 mA/mm at V_{DS} = 10 V and V_{GS} = 0 V.

Even with surface treatments, the surface is not fully recovered, and additional measures must be taken to preserve the semiconductor surface if Al_2O_3 is to be a viable gate dielectric.

This is the subject of ongoing research.

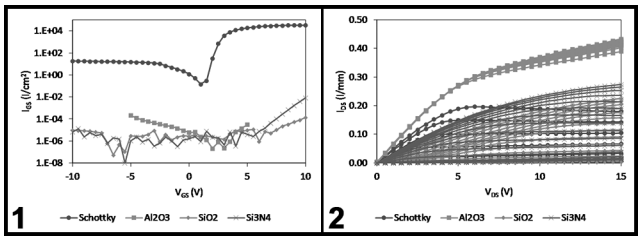

Figure 1, left: *Gate leakage current for Al_2O_3, Si_3N_4, and SiO_2 MISHEMTs compared with conventional Schottky gate HEMT. V_{DS} = 5.5 V.* ***Figure 2, right:*** *Output characteristics for Al_2O_3, Si_3N_4, and SiO_2 MISHEMTs compared with conventional Schottky gate HEMT. The highest curves are at V_{GS} = 0 V, subsequent curves incremented V_{GS} down by 0.5 V. (See pages vi-vii for full color versions of both figures.)*

References:

[1] B. McEwen, I. Mahaboob, E. Rocco, K. Hogan, R. Green, F. Nouketcha, T. Murray, V. Kaushik, A. Lelis, F. Shahedipour-Sandvik. "Investigation of the Effects of Forming Gas Annealing on Al_2O3/GaN Interface," submitted.

[2] B. McEwen, I. Mahaboob, K. Hogan, E. Rocco, V. Meyers, S. Tozier, A. Lelis, R. Green, F. Nouketcha, F. Shahedipour-Sandvik. "Effects of Semiconductor Surface Treatments and Dielectric Anneal on the Electrical Characteristics of GaN-Based Metal-Insulator-Semiconductor Devices." Poster presented at: 13th International Conf on Nitride Semiconductors; 2019 Jul 7-12; Bellevue, WA.

Scissionable Polymer Photoresist for Extreme Ultraviolet Lithography

CNF Project Number: 2751-18
Principal Investigator(s): Christopher Kemper Ober
User(s): Jingyuan Deng, Abhaiguru Ravirajan

Affiliation(s): Materials Science and Engineering, Cornell University
Primary Source(s) of Research Funding: INTEL Corporation
Contact: c.ober@cornell.edu, jd966@cornell.edu, ar2362@cornell.edu
Primary CNF Tools Used: ASML 300C DUV stepper, JEOL-6300 e-beam lithography, P10 profilometer

Abstract:

Extreme ultraviolet (EUV) is one of the most promising methods to create nano-size patterns below 10 nm. Numerous EUV resists have been developed in last decades to accommodate EUV lithography. The main challenge of EUV lithography lies in RLS tradeoff, which specify the tradeoff among resolution (R), line edge roughness (L) and sensitivity (S). In addition, EUV lithography suffers from low photon numbers, which may cause stochastic issues. In this work, we developed chemically amplified chain scissionable polymers to tackle these issues. Polyphthalaldehyde (PPA) based photoresists have been synthesized and their lithographic performance have been investigated.

Summary of Research:

Scissionable polymers are polymers that will depolymerize under different stimuli including acid, base, and free radicals [1]. These polymers have been investigated in the development of photoresists and other degradable materials. This work focuses on the poly(phthalaldehyde), PPA, family of scissionable polymers. The PPA backbone consists of acetal linkages that are very sensitive to acids. Upon exposure to acids, the polymer chain depolymerizes to its corresponding monomers. This depolymerization behavior makes PPAs excellent candidates as photoresist materials. Several new architectures are being explored. For example, PPAs with tethered photoacid generators (PAG)s, which release acid upon irradiation, depolymerize upon exposure followed by a post exposure bake step. The depolymerized monomers in exposed areas could be easily removed using appropriate organic solvents while the unexposed areas remain unchanged. Therefore, both unsubstituted and substituted PPAs may equally serve as a positive tone photoresist.

This study focuses on the development of low exposure dose, sensitive PPA photoresists, which do not suffer from materials stochastic issues related to non-uniformities at nanoscale present in multi-component systems for EUV lithography. In order to improve the lithographic performance of the PPA photoresists, the structure of the polymer backbone as well as photoacid generators (PAG)s are being investigated and tailored for EUV lithography. Aryl sulfonates were prepared as non-ionic PAGs for PPA photoresists [2]. The steric and electronic nature of the aryl sulfonate PAGs can be easily tuned to optimize acid generation efficiency and their compatibility with a polymer photoresist matrix.

Results and Discussions:

The homogenous solution of PPA polymers and PAGs were prepared and spin coated on a silicon wafer. The coated silicon wafers were then exposed using ASML 300C DUV stepper. After exposure, the exposed film was baked and developed. The resulting line-space patterns were characterized using AFM and SEM. The images are shown in Figure 1 and 2, respectively.

Summary:

In summary, preliminary results were obtained with chain scissionable photoresists. With these results in hand, the lithographic performance of newly developed functionalized PPAs will be investigated under DUV, e-beam, and EUV to pursue higher resolution and improved LER.

References:

[1] Yardley, R. E.; Kenaree, A. R.; Gillies, E. R. Macromolecules 2019, 52, 6342.

[2] Sulc, R.; Blackwell, J. M.; Younkin, T. R.; Putna, E. S.; Esswein, K.; DiPasquale, A. G.; Callahan, R.; Tsubaki, H.; Tsuchihashi, T. Proc. SPIE, 2009; 7273, 72733.

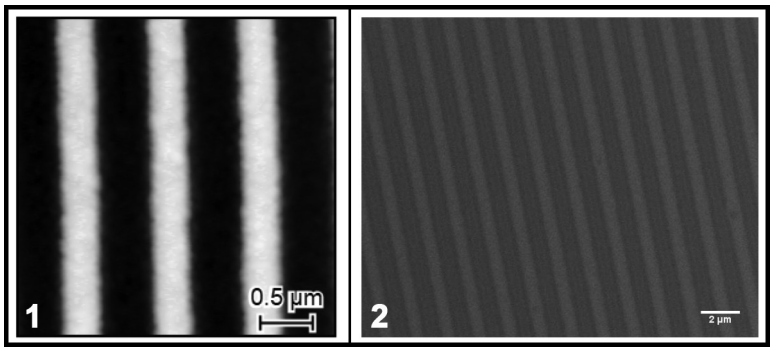

Figure 1, left: *1:1 Line space pattern with feature size 512 nm observed under AFM after exposure of 100 mJ/cm² deep UV exposure. As seen from these figures, the line edge roughness was relatively rough. The acid diffusion, which caused this roughness, could be alleviated by changing the chemical structure of the photoacid generator. Next, we plan to explore the resolution limit of these photoresists with different photoacid generators using e-beam, and EUV. These samples are currently under preparation.*

Figure 2. right: *1:1 Line space pattern with feature size 512 nm observed under SEM after exposure of 100 mJ/cm² deep UV exposure.*

Mitigating Etch-Induced Fencing of Platinum with Sacrificial Layers

CNF Fellows Program

Principal Investigator(s): Vince Genova[1], David Lisham[2]

CNF Fellow: Kyle J. Dorsey[3]

Affiliation(s): 1. Cornell NanoScale Science and Technology Facility, 2. Plasma-Therm LLC, 3. School of Applied and Engineering Physics, Cornell University

Primary Source(s) of Research Funding: Cornell NanoScale Science and Technology Facility

Contact: genova@cnf.cornell.edu, kjd96@cornell.edu

Primary CNF Tools Used: AJA International, GCA AS200 i-line stepper

Abstract:

Lithographic patterning of platinum is challenging because platinum does not readily form volatile etch products. Most approaches toward patterning platinum rely on physical etch mechanisms. Low-energy sputtered platinum has a short mean-free path and high surface mobility, so it readily redeposits on the sidewalls of etch masks. When the etch mask is removed, the sidewall-deposited platinum remains adhered to the wafer in a phenomenon known as "fencing." We describe a lithographic approach to mitigate the effects of platinum etch fencing by utilizing sacrificial layers to lift off the residual fences during etch mask stripping. The central elements of the process are described schematically in Figure 1. A sacrificial layer is prepared with considerable undercut underneath the etch mask as shown in Figure 1(a). The redeposition of platinum from the edge of the feature can be considered a point source. The flux of platinum should then vary as cos θ. Therefore, very little platinum is redeposited underneath the resist, enabling it to be lifted off in solvent.

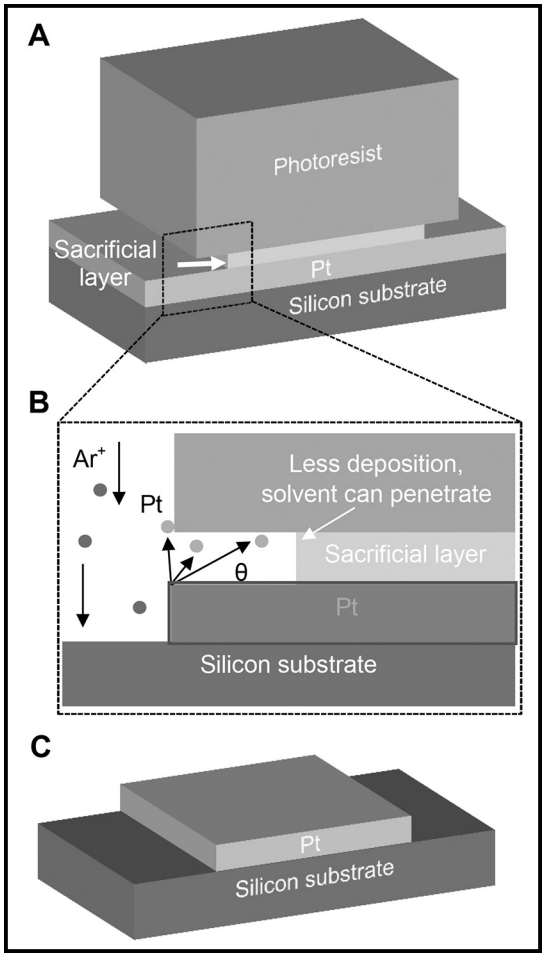

Figure 1: Central elements of the process are described schematically.

Summary of Research:

Platinum films were prepared on silicon wafers by DC sputtering (AJA International). *In situ*, the wafers were cleaned with an Ar plasma, then sequentially coated with 2 nm Ti adhesion layer and 100 nm Pt at 3 mTorr. The sacrificial layer (to be described in subsequent sections) was deposited or spin-coated. The etch mask was patterned by photolithography (GCA AS200 i-line stepper, 5x) in SPR700-1.2 photoresist. The pattern consists of lines and spaces at equal pitch ranging from 0.5 μm to 20 μm. The platinum was etched in an argon ion-milling system at normal incidence with 600V bias. Etching proceeded in 15 second increments with 30 second cooldowns between bursts to prevent overheating. Eight etch/cool cycles were needed to clear through 100 nm of Pt.

The primary sacrificial layer investigated is Microchem LOR resist. This material dissolves in developer solution, producing an undercut profile concurrently with the lithography process. The thickness is controlled by spin-coating and viscosity, and the undercut rate is controlled by soft-bake temperature. After etching, the photoresist was dissolved in heated 1165 stripper (~50°C) with

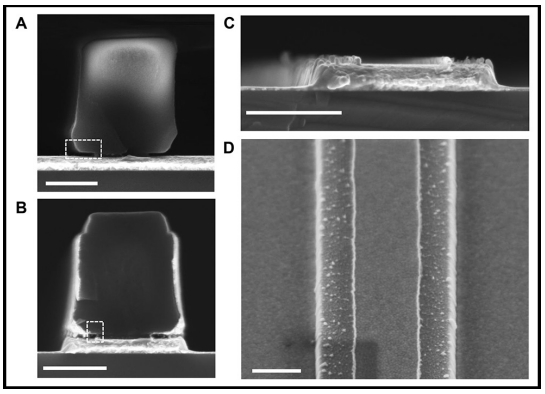

Figure 2: Complete process flow.

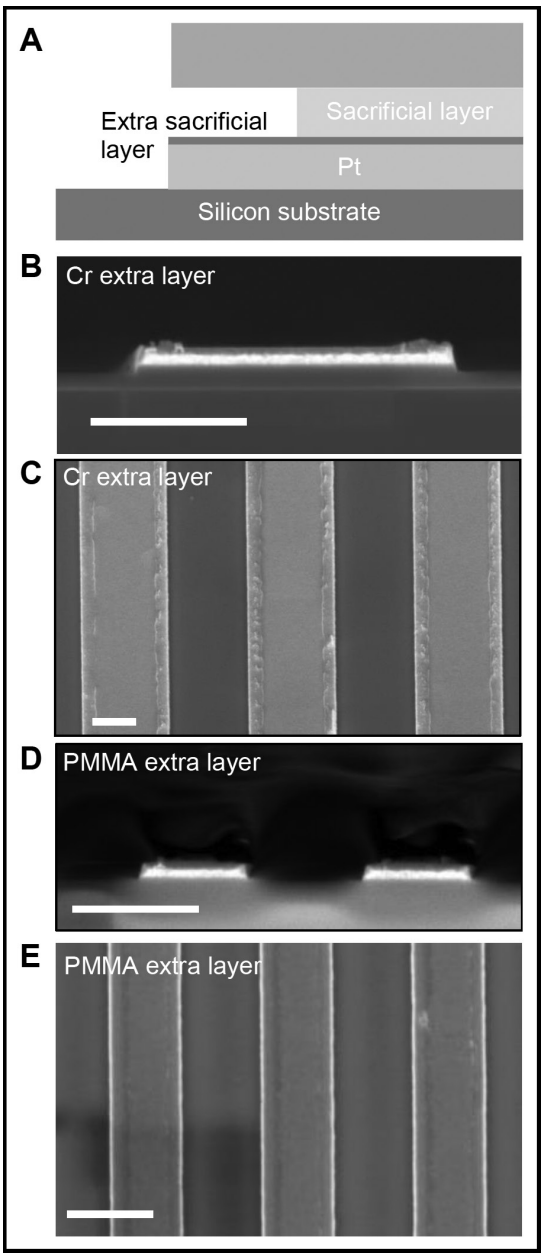

Figure 3; Results of the platinum features after removing the extra sacrificial layer.

ultrasonic agitation for 30 minutes, followed by rinsing in acetone, isopropanol, and DI water.

Results:

We investigated ultra-thin layers of LOR, which simplifies process by having easier to prepare films, eliminating an etch step, and remaining easy to remove. The LOR was prepared by mixing LOR 1A in a 1:1 volumetric ratio with cyclopentanone. This mixture was mixed on a magnetic stir plate for an hour prior to coating. The wafers were spun with this solution at 3500 RPM for 30 seconds and baked at 185°C. At this temperature, the LOR produces an undercut rate of 4 nm/sec in 2.38N developer. The complete process flow with this sacrificial layer is described in Figure 2.

Figure 2a shows the completed structure. The LOR thickness is 40 nm, and the development time produces a 200 nm undercut. After milling, the sidewalls are coated in Pt, as shown in Figure 2b. However, the corners of the completed feature are not coated. This enables separation of the sidewall from the substrate. After removal, the finished structures are shown in cross section in Figure 2c and in angled imaging in Figure 2d. There is some residual platinum, but none of it is thicker than the LOR thickness. Moreover, there are no large regions of retained sidewall as there were for the silicon nitride case.

The remaining Pt particles can be removed by inserting an additional sacrificial layer in between the platinum and the undercut resist, as shown in Figure 3a. The thickness of this additional layer should be very thin as to avoid generation of new, larger fences. It should also not dissolve during photolithography development or resist coating. We investigated two extra sacrificial layers, 10 nm of chromium (sputtered, 3 mTorr) and 10 nm of PMMA.

Figure 3 reports the results of the platinum features after removing the extra sacrificial layer. Figures 3b and 3c show the effects of removing the 10 nm of Cr post-milling with Cr etchant CE-200. There are small additional fences remaining, but fewer large residues compared to the approach without the extra layer. Figures 3d and 3e show the effects of using ultra-thin PMMA films as the extra layer. Compared to the Cr layer, the PMMA films simplify the process since it is removed concurrently with the photoresist in the 1165 bath. This approach has improved residues compared to the Cr-based approach and the process without any extra layers at all.

Future Work:

Future work will focus on further refinement of the sacrificial underlayer approach. It shows promise as a simple route to fence-free platinum etching. An additional interesting experiment involves conformal sacrificial layers deposited over the imaging resist. This conformal layer covers the entire sidewall of the resist pattern. If chosen appropriately, it can lift off the sidewall fences in a single process step. Work is ongoing using ALD-deposited aluminum oxide, which can be deposited conformally at low temperatures and is readily dissolved in TMAH-based photoresist developer.